The molecular mechanism of monovalent cation selectivity in the TRPM5 channel

Callum M. Ives [1,2], **Neil J. Thomson** [1], **Ulrich Zachariae** [1] ✉

[1] Division of Computational Biology, School of Life Sciences, University of Dundee, Dow Street, Dundee, DD1 5EH, UK.

✉ **For correspondence:** u.zachariae@dundee.ac.uk

Present address: [2] Department of Chemistry and Hamilton Institute, Maynooth University, Maynooth, Kildare, Ireland.

Data availability: MD simulation inputs and analysis scripts used for this study are deposited in a public GitHub repository, available at: https://github.com/cmives/Na_selectivity_mechanism_of_TRPM_channels.

Funding: CMI was supported by the Medical Research Council [grant number MR/N013735/1], and NJT was supported by the UKRI Biotechnology and Biological Sciences Research Council (BBSRC) [grant number BB/M010996/1].

Competing interests: The author declare no competing interests.

Abstract

A key capability of ion channels is the facilitation of selective permeation of certain ionic species across cellular membranes at high rates. Due to their physiological significance, ion channels are of great pharmaceutical interest as drug targets. The polymodal signal-detecting Transient Receptor Potential (TRP) superfamily of ion channels form a particularly promising group of drug targets. While most members of this family permeate a broad range of cations, TRPM4 and TRPM5 are unique due to their strong monovalent-selectivity and impermeability for divalent cations. Here, we address the mechanistic basis for their unique monovalent-selectivity. We present results from *in silico* electrophysiology simulations of cation permeation through the TRPM5 channel, showing that monovalent cations permeate by a co-operative, distant knock-on mechanism between cation binding sites in the extracellular pore vestibule and the pore cavity. By contrast, divalent cations experience an energy barrier within the pore cavity, which inhibits their permeation via a knock-on mechanism.

Introduction

The translocation of ions across cellular and organellar membranes via ion channels is essential to ensure cellular ionic homeostasis and provides a key pathway of intra- and intercellular communication. Ion channels catalyse the permeation of ions across the membrane up to an order of 10^6 ions per second, while at the same time often displaying strict selectivity for particular ionic species ***Roux*** (***2017***). The transient receptor potential (TRP) superfamily of ion channels comprises a large group of cation-selective channels that are implicated in a wide range of physiological processes ***Ramsey et al.*** (***2006***); ***Khalil et al.*** (***2018***). Due to their physiological importance, TRP channels are associated with a large number of pathological conditions ***Nilius*** (***2007***), including in the aetiology of several rare, genetic conditions. Therefore, many members of the TRP channel superfamily constitute major pharmaceutical target proteins ***Moran*** (***2018***); ***Koivisto et al.*** (***2022***).

Within the TRP channel superfamily, TRPM (transient receptor potential melastatin) channels form the largest subfamily, consisting of eight members (TRPM1-8) ***Nilius and Owsianik*** (***2011***); ***Samanta et al.*** (***2018***). TRPM channels assemble as homotetramers, in which each subunit provides six transmembrane helices (S1-S6), a cytosolic *N*-terminus domain composed of four melastatin homology regions, and a cytosolic *C*-terminus coiled-coil domain ***Hilton et al.*** (***2019***); ***van Goor et al.*** (***2020***). In keeping with most members of the TRP superfamily, TRPM channels are described as being cation non-selective, that is, they conduct cations but do not differentiate substantially between cationic species. However, in the TRPM subfamily, TRPM4 and TRPM5 are exceptions to this observation, since both channels are selective for monovalent cations and impermeable to divalent cations ***Owsianik et al.*** (***2006***). TRPM4 and TRPM5 are therefore the only members of the wider TRP superfamily to display selectivity for monovalent cations.

Although TRPM4 and TRPM5 are close homologues as they share a high degree of sequence homology and have similar biophysical characteristics, there are some variations in their activation mechanisms. For example, while both channels are activated by intracellular Ca^{2+} concentrations, TRPM5 is approximately 20-fold more sensitive to Ca^{2+} than TRPM4 ***Ullrich et al.*** (***2005***). TRPM5 signalling has been implicated in the taste of sweet, bitter, and umami tastes in type II taste bud cells ***Pérez et al.*** (***2002***); ***Zhang et al.*** (***2003***), and in the secretion of insulin by pancreatic β-cells ***Brixel et al.*** (***2010***); ***Colsoul et al.*** (***2010***). Consequently, TRPM5 is a potential drug target for a number of conditions, including metabolic conditions such as type II diabetes mellitus ***Vennekens et al.*** (***2018***). Several structures of the TRPM4 and TRPM5 channel have been published to date, however an open-state structure has only been solved for TRPM5 ***Ruan et al.*** (***2021***).

In the present work, we set out to characterise the cation permeation mechanism of the TRPM5 channel, focusing in particular on the basis for its monovalent cation selectivity. We conducted atomistic molecular dynamics (MD) simulations and *in silico* electrophysiology of the open-state structure of *Danio rerio* TRPM5 ***Ruan et al.*** (***2021***), using Na^+, K^+, and Ca^{2+} ions as examples for monovalent and divalent biological ions. In total, we recorded 568 ion permeation events within 17.25 μs of aggregated time from *in silico* electrophysiology simulations. Our findings suggest a new mechanism of selectivity that is based on an extra binding site for monovalent cations in the channel's cavity, rather than on differentiating ions in the selectivity filter. Conduction of monovalent ions is therefore a synergistic process incorporating co-operativity between multiple binding sites, whereas the conduction of divalent ions is inefficient in comparison.

Methods & Materials

TRPM5 system construction

A truncated TRPM5 simulation system consisting of the membrane-domain of the channel was constructed by using residues 698-1020, including the *N*-acetyl-β-D-glucosamine of the glycosylated N921 residue, of the *Danio rerio* TRPM5 structure ***Ruan et al.*** (***2021***). We also modelled the bound Ca^{2+} cations occupying the Ca_{TMD} binding site, which have been proposed to be implicated in Ca^{2+}-dependent activation of TRPM5. The system was built using the CHARMM-GUI server ***Jo et al.*** (***2008***). The charged *N*- and *C*-terminal residues were neutralised by capping with acetylated

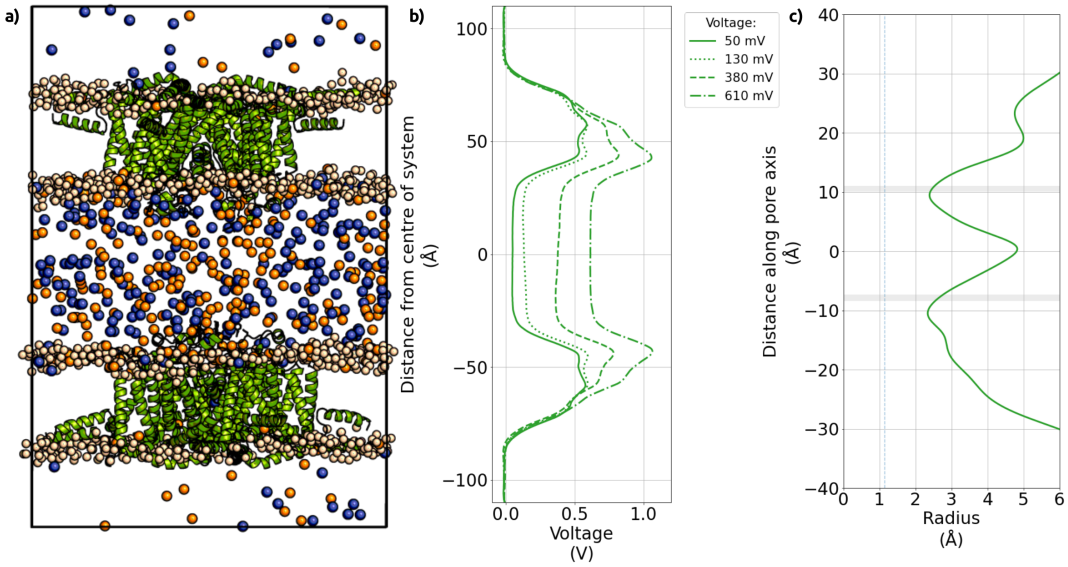

Figure 1. Structure and membrane voltage of CompEL simulations of TRPM5. **a)** Snapshot of the CompEL system showing the TRPM5 pore domain of *Danio rerio* used in this study inserted into a double bilayer simulation system in an anti-parallel fashion so that both proteins experience identical voltage polarity. Cations within the aqueous compartments are shown as spheres (orange: calcium; blue: sodium), highlighting the 9:1 ion concentration gradient between the compartments. **b)** The CompEL charge differences we applied across the aqueous compartments (Δq) resulted in transmembrane voltages of ∼ -50 mV, -130 mV, -380 mV, and -610 mV in addition to the concentration gradient. **c)** Average pore radius of TRPM5 along the pore axis from MD simulations. The regions in grey shade represent the average positions of the major pore constrictions in TRPM5, formed by Q906 (*upper* gate) and I966 (*lower* gate). The dashed line indicates the radius of a completely dehydrated Ca^{2+} ion for comparison.

(ACE) and *N*-methylamidated (CT3) groups, respectively. All missing non-terminal residues were modelled ***Jo et al.*** (***2014***).

The structure was aligned in the membrane using the PPM server ***Lomize et al.*** (***2012***), and inserted into a 1-palmitoyl-2-oleoyl-sn-glycerol-3-phosphocholine (POPC) bilayer of 160 x 160 Å size using the CHARMM-GUI membrane builder ***Jo et al.*** (***2007***); ***Wu et al.*** (***2014***), and then solvated. Ions were added using GROMACS 2020.2 ***Abraham et al.*** (***2015***); ***Lindahl et al.*** (***2020***) to neutralise any system charges and add ions to a concentration of either 150 mM NaCl, 150 mM KCl, 150 mM $CaCl_2$ (referred to as mono-cationic solutions), or a mixture of 75 mM NaCl and 75 mM $CaCl_2$ (referred to as di-cationic solutions). In the case of simulations containing Ca^{2+}, the standard CHARMM36m Ca^{2+} ions were then replaced with the multi-site Ca^{2+} of Zhang *et al.* ***Zhang et al.*** (***2020***). This multi-site model has used been used to investigate Ca^{2+} permeation in a number of channels, including including the type-1 ryanodine receptor ***Zhang et al.*** (***2020***); ***Liu et al.*** (***2021***), AMPA receptors ***Schackert et al.*** (***2022***), the E protein of SARS-CoV-2 ***Antonides et al.*** (***2022***), and TRPV channels ***Ives et al.*** (***2022***); ***Liu and Song*** (***2022***).

Molecular dynamics simulations details

All simulations were performed using GROMACS 2020.2 ***Abraham et al.*** (***2015***); ***Lindahl et al.*** (***2020***) or GROMACS 2022 ***Bauer et al.*** (***2022***), and the CHARMM36m force field for the proteins, lipids, and

Table 1. Summary of simulations performed in this study.

Protein	Transmembrane voltage methodology	Voltage	Ion solution	Simulation duration
TRPM5	CompEL (anti-parallel)	-50 mV	75 mM NaCl + 75 mM $CaCl_2$	3 x 500 ns
		-130 mV	75 mM NaCl + 75 mM $CaCl_2$	3 x 500 ns
		-380 mV	75 mM NaCl + 75 mM $CaCl_2$	3 x 500 ns
		-610 mV	75 mM NaCl + 75 mM $CaCl_2$	3 x 500 ns
	External applied field	-50 mV	150 mM NaCl	3 x 250 ns
			150 mM $CaCl_2$	3 x 250 ns
		-200 mV	150 mM NaCl	3 x 250 ns
			150 mM $CaCl_2$	3 x 250 ns
		-340 mV	150 mM NaCl	3 x 250 ns
			150 mM KCl	3 x 250 ns
			150 mM $CaCl_2$	3 x 250 ns

ions ***Huang et al.*** (***2016***). The TIP3P water model was used to model solvent molecules ***Jorgensen et al.*** (***1983***). The system was minimised and equilibrated using the suggested equilibration inputs from CHARMM-GUI ***Lee et al.*** (***2016***). In brief, the system was equilibrated using the NPT ensemble for a total time of 1.85 ns with the force constraints on the system components being gradually released over six equilibration steps. The systems were then further equilibrated by performing a 15 ns simulation with no electric field applied. To prevent closing of the lower-gate of the pore, harmonic restraints were applied to maintain the distance between the α-carbon atoms of the lower gate I966 residue of each respective chain. The temperature was maintained at 310 K using the Nose-Hoover thermostat ***Evans and Holian*** (***1985***) and the pressure was maintained semi-isotropically at 1 bar using the Parrinello-Rahman barostat ***Parrinello and Rahman*** (***1981***). Periodic boundary conditions were used throughout the simulations. Long-range electrostatic interactions were modelled using the particle-mesh Ewald method ***Darden et al.*** (***1993***) with a cut-off of 12 Å. The LINCS algorithm ***Hess et al.*** (***1997***) was used to constrain bonds with hydrogen atoms. Hydrogen mass re-partitioning (HMR) of the system was used to allow the use of 4-fs time steps in simulations of NaCl solutions. The multi-site Ca^{2+} model used for simulations of $CaCl_2$ however is incompatible with a 4-fs time step, and therefore any simulations including Ca^{2+} cations were performed with HMR but at a time step of 2-fs.

A summary of all simulations is summarised in Table 1, and can be found in more detail in Tables S1 and S2.

CompEL simulations

We employed the computational electrophysiology (CompEL) protocol ***Kutzner et al.*** (***2011***, 2016) of GROMACS to create a transmembrane voltage and to drive ion permeation. We performed this using an anti-parallel double bilayer system, so that both channels experienced the same voltage polarity, with negative polarity in the intracellular region. We performed simulations in a di-cationic solution of 75 mM NaCl and 75 mM $CaCl_2$ with a range of ionic imbalances (Δq), resulting in simulations with voltages of ∼ -50 mV, -130 mV, -380 mV, and -610 mV. To further drive cation permeation, we also created a neutral ion concentration gradient of 9:1 between the extracellular and intracellular solutions (Figure 1). All CompEL simulations were 500 ns long and repeated three times for each system, resulting in an aggregated simulation time of 3 µs per voltage due to the double channel nature of these simulations.

External applied field simulations

In addition to CompEL simulations, we also performed simulations in a mono-cationic simulation of 150 mM NaCl, 150 mM KCl, 150 mM $CaCl_2$, using the method of ***Aksimentiev and Schulten*** (***2005***) to produce an external electric field. These simulations had an E_0 of either -0.03, -0.0175, or -0.0044 V nm^{-1}, resulting in a transmembrane voltage of ∼340 mV, 200 mV, or 50 mV, respectively, with negative polarity in the intracellular region. All applied field simulations were 250 ns long and repeated three times for each system.

Simulation analysis

Analysis of MD trajectory data was performed using in-house written Python scripts, utilising GROMACS modules ***Abraham et al.*** (***2015***); ***Lindahl et al.*** (***2020***), the SciPy library of tools ***Oliphant*** (***2007***); ***Pérez and Granger*** (***2007***); ***Millman and Aivazis*** (***2011***); ***Van Der Walt et al.*** (***2011***), and MDAnalysis ***Michaud-Agrawal et al.*** (***2011***); ***Gowers et al.*** (***2016***). Analysis of the pore architecture was performed using CHAP ***Rao et al.*** (***2019***). All plots were generated in Python using Matplotlib ***Hunter*** (***2007***) and Seaborn ***Waskom et al.*** (***2018***). All MD inputs and analysis scripts used for this study are deposited in a public GitHub repository, available at: https://github.com/cmives/Na_selectivity_mechanism_of_TRPM_channels.

Calculating conductance and selectivity from *in silico* electrophysiology experiments

The conductance of the channels (C_{ion}) was calculated according to Equation 1, where N_p is the number of permeation events, Q_{ion} is the charge of the permeating ion in Coulomb, t_{traj} is the length of the trajectory, and V_{tm} is the transmembrane voltage. The mean conductance and standard error were calculated from overlapping 50 ns windows of the trajectory.

$$C_{ion} = \frac{N_p \times Q_{ion}}{t_{traj} \times V_{tm}} \tag{1}$$

The selectivity (P_{Na}/P_{Ca}) from the di-cationic CompEL simulations was calculated as the ratio between the total sum of Na^+ permeation events and the total sum of Ca^{2+} permeation events across all simulations.

Identification of cation binding sites from MD simulations of TRPV channels

Cation binding sites were identified by plotting timeseries of each permeating ion with respect to their position along the pore axis. To further validate these positions, a 3D density mesh was generated for cations within 10 Å of the protein. This analysis was performed on a trajectory of concatenated three-fold replicated 500 ns simulations from mono-cationic simulations with a voltage of ∼ -50 mV produced by the CompEL method.

Characterising permeation co-operativity through mutual information using SSI from PENSA

To characterise the level of co-operativity in the knock-on permeation mechanisms of the TRPM5 channel, we used PENSA to calculate the state-specific information (SSI) shared between discrete state transitions in the occupancy distributions of both of the binding sites ***Thomson et al.*** (***2021***); ***Vögele et al.*** (***2022***). The methodology used is the same as that described in detail in our previous work ***Ives et al.*** (***2022***).

In brief, a timeseries distribution with a timestep of 20 ps for each binding site was obtained, whereby for each frame, if an ion occupied the binding site then this ion's atom ID number was recorded, whereas if the binding site was unoccupied, an ID of -1 was recorded. We then quantified by mutual-information based SSI whether ion transitions at one site were coupled to ion transitions at the adjacent site. To account for statistical noise that can arise from even independent distributions ***McClendon et al.*** (***2009***); ***Pethel and Hahs*** (***2014***), we calculated a statistical threshold which we subtracted from our measured values to resolve the excess mutual information, or excess SSI ($exSSI$).

Results

Cation conductance of the TRPM5 channel in di-cationic solutions

We performed *in silico* simulations of *Danio rerio* TRPM5 ***Ruan et al.*** (***2021***) embedded in a POPC lipid bilayer with a di-cationic ionic solution of 135 mM NaCl and 135 mM $CaCl_2$ in the central dense aqueous compartment, and 15 mM NaCl and 15 mM $CaCl^2$ in the outer diluted aqueous compartments (Figure 1). An anti-parallel CompEL setup was used to produce a bio-mimetic transmembrane voltage of ∼ -50 mV, as well as higher voltages of -130 mV, -380 mV and -610 mV to increase the number of permeation events and improve the statistics of our analyses (Figure 1). In addition to the membrane voltages, the 9:1 ion concentration gradient between the middle and the outside bulk compartment also drove ion permeation.

Our simulations under ion and voltage gradients showed a continuous flow of permeating ions, resulting in a total of 374 permeation events across all investigated simulation conditions. Despite the ion gradient providing an additional driving force for permeation alongside the voltage, the calculated conductances from our *in silico* electrophysiology simulations, in a range between 7 and 38 pS (Table 2), are generally in good agreement with the published conductance values of 23–25 pS from *in vitro* electrophysiology in NaCl based solutions ***Hofmann et al.*** (***2003***); ***Prawitt et al.*** (***2003***).

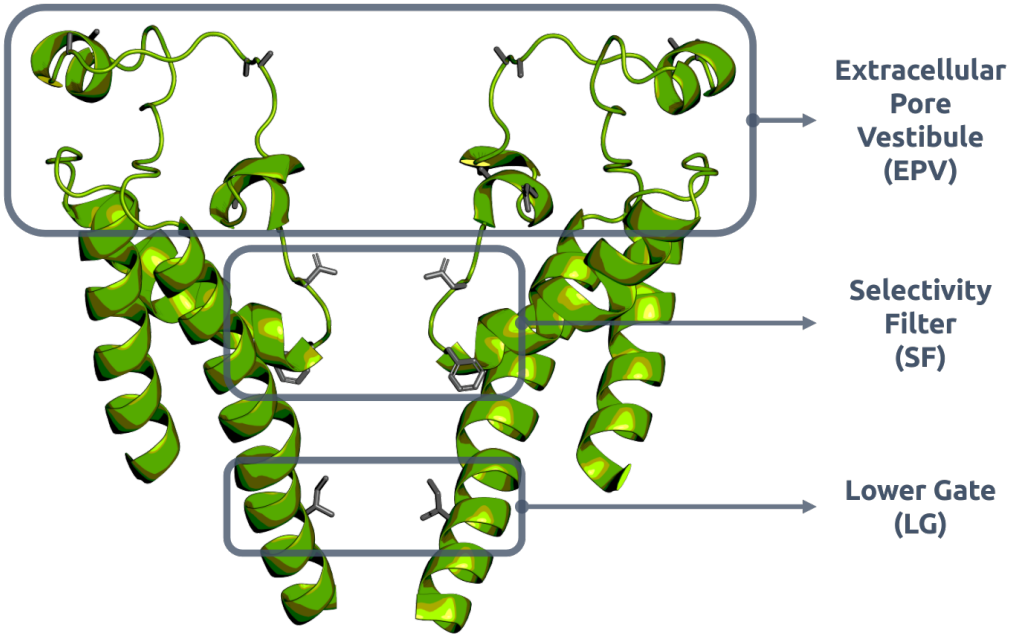

Figure 2. Overview of the structure of the TRPM5 channel of *Danio rerio* used in this work (two of the four subunits are omitted for clarity). TRPM5 has a short, three-residue selectivity filter (SF) consisting of Q906, G905, and F904. The hydrophobic lower gate (LG) of TRPM5 is formed by I966. In this study, the pore is defined as the region between the the two constrictions of the channel, namely Q906 of the SF and I966 of the lower gate. Above the pore is the extracellular pore vestibule, which contains a number of acidic residues, such as 910, E911, D919, D920, D925, and E928. All residues mentioned by name are displayed as grey sticks.

Low-voltage simulations in di-cationic solutions show the exclusive permeation of Na^+ through TRPM5

At the lowest voltages of ∼ -50 mV and -130 mV, we observe complete Na^+-selectivity in mixed solutions, with no recorded Ca^{2+} permeation during an accumulated simulation time of 1.5μs, while in the same time span, 15 Na^+ ions traverse the TRPM5 pore, in accordance with its general conductance level (Table 2).

Analysis of the pore architecture of TRPM5 showed no major conformational changes throughout the course of the simulations. The TRPM5 pore possesses two main constrictions: an upper constriction formed by the sidechains of Q906 of the three-residue selectivity filter (SF), and a lower constriction formed by by the sidechains of I966 of the lower gate (Figure 1). A minor constriction can also be observed ∼13 Å above the SF, in the extracellular pore vestibule (EPV) (Figure 2). This constriction is formed by the loop between the pore helix (PH) and the S6 helix.

In our simulations at -50 mV and -130 mV, Na^+ cations first enter the EPV region of the TRPM5 pore, where they show a broad association. Permeating Na^+ cations then traverse the SF rapidly, and enter the pore cavity. They spend a substantial amount of time occupying the cavity before passing through the lower gate and exiting the pore at the intracellular face.

Figure 3. 3D density map of Ca^{2+} cations around the EPV and SF of TRPM5. The density of Ca^{2+} ions was calculated from concatenated trajectories of TRPM5 in a di-cationic solution under a transmembrane voltage of ∼ -50 mV generated by the CompEL method. A major density maxima is seen within the EPV, where Ca^{2+} bind and associate. Occasionally, a Ca^{2+} cation approaches the SF, however is not able to traverse past through the SF at bio-mimetic voltages. The sidechains of Q906 of the SF and I966 of the lower gate are shown as sticks for clarity (*grey*).

As opposed to monovalent Na^+, Ca^{2+} ions did not readily enter the inner pore of TRPM5 during the course of the simulations. Ca^{2+} cations chiefly occupied the EPV region at the extracellular entrance (see Figure 2). 3-D density maps of Na^+ and Ca^{2+} ions further confirmed this observation (Figure 3). The maps show substantial Ca^{2+} density in the EPV, particularly near the acidic residues on the loop between the PH and the S6 helix, namely: E910, E911, D919, D920, D925, and E928. We observed that Ca^{2+} ions occasionally migrate from the EPV toward the pore, however they are blocked from entering the cavity at the SF, particularly at the constriction formed by Q906 (Figure 3).

The ion selectivity of TRPM5 is strongly voltage-dependent

As the membrane voltage is increased, the Na^+ selectivity (P_{Na}/P_{Ca}) in the CompEL simulations is diminished (Table 2). At a voltage of both ∼ -50 mV and ∼ -130 mV, we observe complete Na^+-selectivity, with no Ca^{2+} permeation events in any of the simulations. At a voltage of ∼ -380 mV, the *in silico* electrophysiology simulations continue to display slightly Na^+-selective permeation; how-

Table 2. Calculated conductances and selectivities from CompEL simulations of ion permeation in the TRPM5 channel. Mean inward conductances and standard error of the mean (SEM) were calculated from overlapping 50 ns windows from three-fold replicated 500 ns simulations of an anti-parallel double bilayer system. Mean selectivity ratios of Na^+ and Ca^{2+} permeation events and SEM were calculated from three-fold replicated 500 ns simulations. The raw number of permeation events for each cation is displayed in brackets below the respective conductance value.

Conc. gradient	Voltage (mV)	Conductance (pS)				P_{Na}/P_{Ca}
		Na^+	Ca^{2+}	Cl^-	Overall	
135 mM : 15 mM	**50**	16 ± 3.1 (*15*)	0 ± 0.0 (*0*)	0 ± 0.0 (*0*)	16 ± 3.1	∞
	130	7 ± 1.3 (*18*)	0 ± 0.0 (*0*)	0 ± 0.0 (*0*)	7 ± 1.3	∞
	380	4 ± 0.5 (*32*)	5 ± 0.8 (*19*)	0 ± 0.1 (*1*)	9 ± 1.0	1.9 ± 0.41
	610	10 ± 0.9 (*115*)	29 ± 2.5 (*168*)	-1 ± 0.2 (*6*)	38 ± 3.1	0.8 ± 0.13

ever, when the voltage is further increased to ~ -610 mV, Na^+-selectivity is lost. Furthermore, higher voltage simulations also yielded a small number of Cl^- permeation events, with anions permeating through to the extracellular solution.

Our findings indicate a strongly voltage-dependent energy surface for permeation across the TRPM5 pore, suggesting relatively weak cation binding sites within the pore domain. These observations are reminiscent of the effects seen for high voltage simulations of the related TRPV channel subfamily, in which Ca^{2+}-selectivity for TRPV5 and TRPV6 was reduced at higher-voltage regimes ***Ives et al.*** (***2022***).

In order to explore the ion permeation dynamics in TRPM5 and their underlying energetic properties further, we aimed to enhance the sampling of both Na^+ and Ca^{2+} permeation events, while at the same time maintain a Na^+-selective voltage range. We thus selected a voltage of ~ -340 mV as a compromise for studying permeation in mono-cationic solutions to ensure a sufficient number of traversals of both Ca^{2+} and Na^+ while remaining within the monovalent-selective regime.

Mechanistic insights into ion permeation in TRPM5 from mono-cationic solutions

We next conducted *in silico* electrophysiology simulations using an applied external electric field of ~ -340 mV across the membrane to investigate the permeation mechanism of Na^+ and Ca^{2+} ions *in mono-cationic solutions*, as well as K^+ ions, with sufficient sampling efficiency (Table 3). As shown in Figure 4, there is a clear difference between the behaviour of monovalent cations in the channel, such as Na^+ and K^+ ions, and the divalent Ca^{2+} ions.

Whereas Na^+ and K^+ ions occupy the central cavity of the channel for most of the simulated

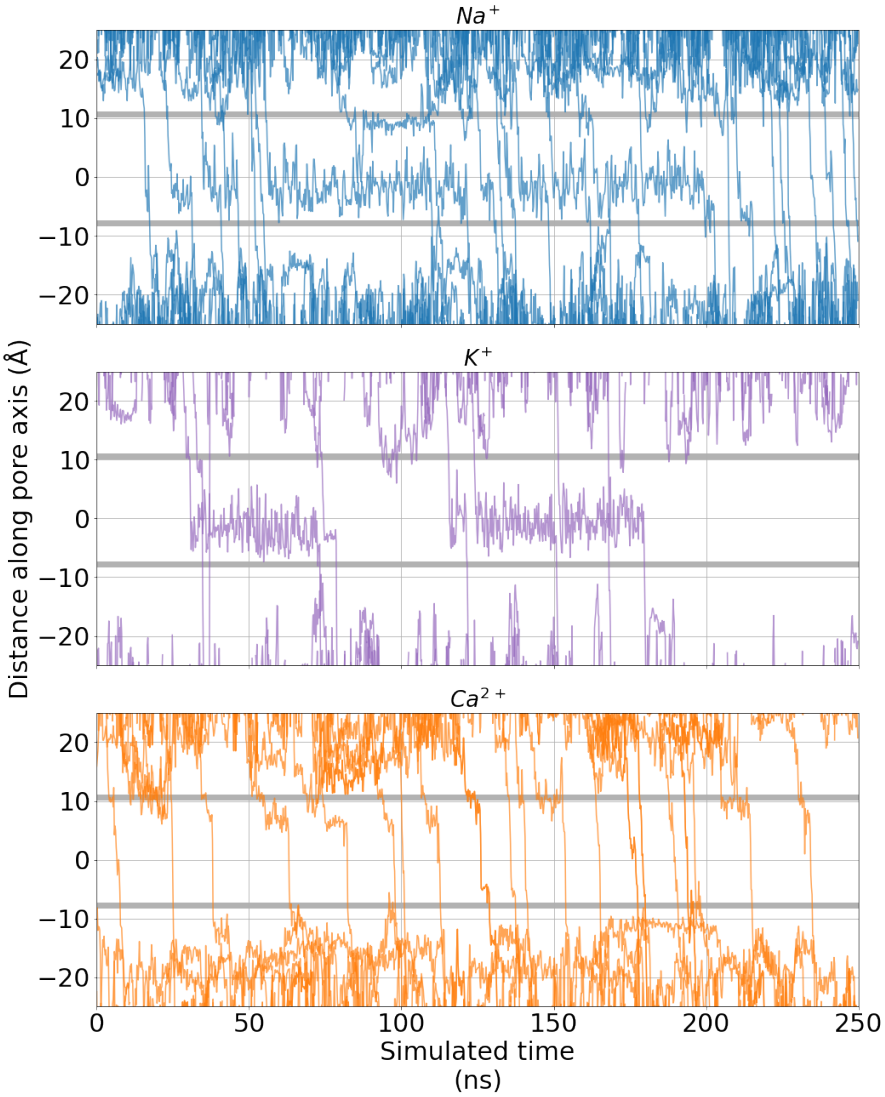

Figure 4. Exemplar permeation traces of the z-coordinate of permeating cations over time. The permeation traces of Na^+ (*blue, top*), K^+ (*purple, middle*), and Ca^{2+} (*orange, bottom*) are plotted from simulations performed in a mono-cationic solution with an external applied electric field. The shaded grey regions represent the average position of the pore constrictions formed by Q906 (*upper*) and I966 (*lower*). Simulation data is from simulations performed in a mono-cationic solution with an external applied electric field producing a voltage of ∼ -340 mV. Please note, only cations that fully permeate through the pore within the 250 ns simulation are shown in the plot.

time, any permeating Ca^{2+} ions traverse the inner cavity rapidly, not showing any apparent immobilisation within the cavity. Despite occupying the cavity for extended periods of time, Na^+ and K^+ ions do not seem to bind to a particular binding site or residue within the cavity, but explore nearly the entire cavity volume before they permeate to the intracellular side.

Looking at the density of ions along the pore axis, and using the negative logarithmic density as

Table 3. Calculated conductances from applied field simulations of ion permeation in the TRPM5 channel. Mean inward conductances and standard error of the mean (SEM) were calculated from overlapping 50 ns windows from three-fold replicated 500 ns simulations of a single bilayer system. The raw number of permeation events for each cation is displayed in brackets below the respective conductance value.

Voltage (mV)	Ion solution	Conductance (pS)
-50	**150 mM NaCl**	19 ± 6.7 (*4*)
	150 mM $CaCl_2$	0 ± 0.0 (*0*)
-200	**150 mM NaCl**	17 ± 3.1 (*15*)
	150 mM $CaCl_2$	9 ± 3.8 (*4*)
-340	**150 mM NaCl**	52 ± 5.6 (*83*)
	150 mM KCl	21 ± 4.2 (*34*)
	150 mM $CaCl_2$	85 ± 5.0 (*54*)

an estimate for the underlying free energy profile at the non-equilibrium permeation conditions we probed under membrane voltage, it can be seen that the cavity region forms a shallow, wide energy minimum for the monovalent cations, whereas Ca^{2+} ions experience a small energy barrier in the same region (Figure 5). In contrast, both monovalent and divalent ions show binding to a shallow binding site, corresponding to the EPV. Both ion types experience a slight energy barrier to permeation near the intracellular channel exit.

We conducted additional simulations using an applied external electric field of differing magnitudes. Notably, whereas the main features of the ion density and free energy estimates occur across all tested voltages, Ca^{2+} is increasingly excluded from the cavity, and is no longer able to enter into the cavity at the lowest voltage of -50 mV during the time span of our simulations (Figure S1). This shows again that the ion selectivity of TRPM5 is strongly voltage-dependent. We next aimed to elucidate the molecular foundations of this behaviour and selectivity in general.

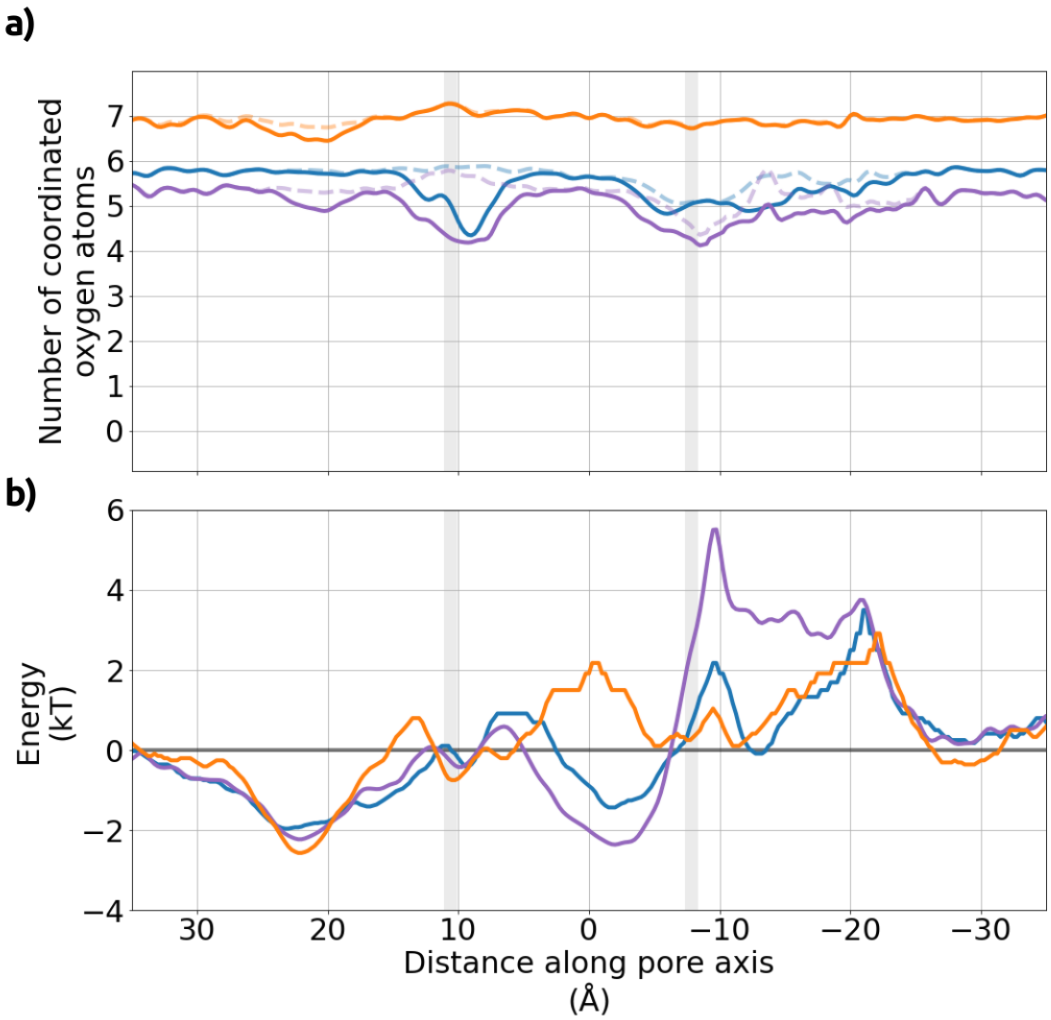

Figure 5. Solvation and PMF profiles of Na^+ (*blue*), K^+ (*purple*) and Ca^{2+} (*orange*) cations through the TRPM5 pore. These simulations were performed in a mono-cationic solution, with an external applied field used to produce a transmembrane voltage of ∼ -340 mV. **a)** The mean number of oxygen atoms of water molecules (*solid line*) and of any oxygen atoms of any molecule (*dashed line*) within 3 Å of each permeating cation is plotted. **b)** Negative logarithmic density profiles of permeating cations along the pore of the TRPM5. The logarithmic ion densities represent quasi-free energies (with a nominal unit of kT). Density minima reflect stably bound ions (i.e. binding sites), while maxima indicate barriers between the binding sites. The location of the pore constrictions formed by Q906 (*upper*) and I966 (*lower*) are represented as grey regions. Both plots have been smoothed using a Gaussian filter with a sigma value of 2.

Solvation profiles of cations during channel permeation

To probe if cation desolvation played a part in yielding selective permeation, especially at the narrowest constriction near Q906 of the SF, we calculated the number of water oxygen atoms within a 3 Å radius of cations, representing their first solvation shell (Figure 5). The desolvation of permeating ions has previously been reported as one important mechanism to ensure ion selectivity in some channels. Differences in the desolvation energies of permeating ions provide a thermody-

namic penalty which can underpin more favourable permeation of an ionic species over another. This mechanism of ion selectivity by desolvation is suggested to be particularly pertinent in K^+ channels ***Köpfer et al.*** (***2014***); ***Kopec et al.*** (***2018***).

In the bulk solution of the simulated systems, Na^+, K^+, and Ca^{2+} ions show the expected water coordination number of their solvation shells. As both Na^+ and K^+ ions enter the pore of TRPM5, they are partially desolvated by Q906, the side chain displacing 1–2 water molecules from the first solvation shell of the ion. After traversing the constriction at Q906, these monovalent ions are then re-solvated in the pore cavity, before again being partially de-solvated at the hydrophobic lower gate formed by I966. By contrast, the rapidly permeating Ca^{2+} ions do not show any significant desolvation when they cross the SF or hydrophobic lower gate of TRPM5.

Furthermore, the solvation profiles of permeating cations show an additional region of differing desolvation within the EPV highlighted previously (Figure 2). In this region, Ca^{2+} and K^+ ions are partially desolvated, indicating closer interactions with the acidic residues in the EPV region. By contrast, Na^+ cations do not show any desolvation there.

We observe similar similar solvation profiles for permeating cations in both our external applied electric field simulations in a mono-cationic solution (Figure S2), and our CompEL simulations in a di-cationic solution (Figure S3), at a range of voltage magnitudes.

Summarising, these data suggest that ion desolvation in the SF is not a major factor in achieving selectivity for monovalent cations. Since both monovalent and divalent cations occupy the EPV, filtering for monovalent ions must occur later in the permeation pathway. However, Ca^{2+} ions are not desolvated when they reach the inner cavity.

As the energetic penalty for desolvating Ca^{2+} is far larger than for Na^+ and K^+ ***Marcus*** (***1991***), the observed desolvation profile cannot explain the deselection of Ca^{2+} ions for further traversal of the cavity and pore.

Selectivity for monovalent cations is based on permeation co-operativity between two binding sites

We hypothesised that the permeation mechanism of monovalent ions, such as Na^+, may be more efficient than that of Ca^{2+} ions due to the presence of an additional binding site for monovalent cations in the internal channel cavity. In previous work, we have developed a mutual-information based assessment of the permeation co-operativity across multiple ion binding sites in channels, which we termed state-specific information (SSI; ***Thomson et al.*** (***2021***); ***Ives et al.*** (***2022***); ***Vögele et al.*** (***2022***)). In brief, SSI quantifies the probability that a state change in one binding site, i.e. a change from binding an ion to being vacant upon ion permeation, is correlated to a similar state change in a second binding site, in which case the unbinding events are coupled to one another.

We applied the SSI approach to ion conduction in TRPM5, focusing on the pair of binding sites at the EPV and the channel cavity (see Figure 2). These two binding sites are shallow but locate directly to the main pore axis; in addition, they show moderate to high occupancy with monovalent cations, respectively (Figure 6). By using SSI, we found that both Na^+ and K^+ ions display a high level of correlation between binding and unbinding at the two successive sites, whereas the permeation of Ca^{2+} ions shows only a low degree of correlation (Figure 6). This means that a distant

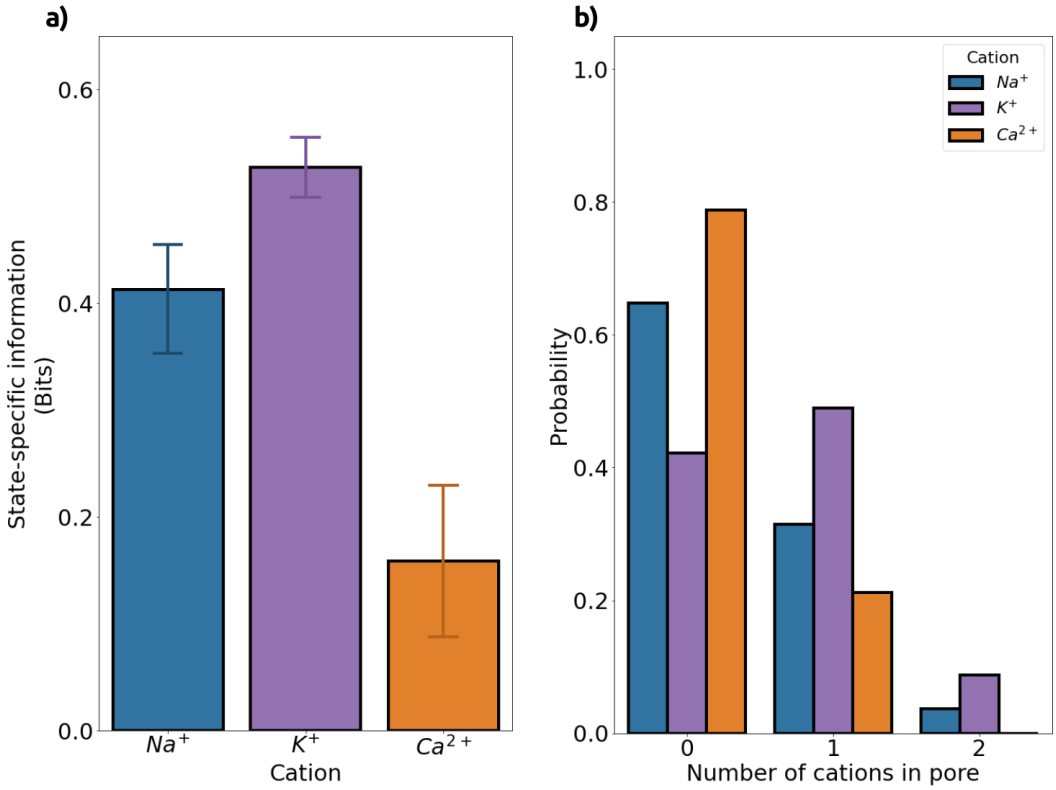

Figure 6. State-specific information (SSI) of cation transitions between binding sites and the average number of each cation within the pore of TRPM5. **a)** Excess state-specific information ($exSSI$) between the EPV and pore cavity ion binding sites quantifies the degree of co-operativity in the permeation mechanisms of Na^+ (*blue*), K^+ (*purple*), and Ca^{2+} (*orange*) ions. The mean exSSI and SEM between transitions from the two binding sites were calculated from simulations performed in mono-cationic simulations with an external applied electric field producing a voltage of ∼ -340 mV. **b)** The mean probability for the number of each cationic species within the pore was calculated from non-overlapping 50 ns windows from three-fold replicated 250 ns simulations, with the pore defined as the region between the constrictions formed by Q906 and I966.

knock-on mechanism is in operation between incoming monovalent ions, which bind transiently at the SF as well as over substantial time spans within the cavity. In other words, the cavity serves as a reservoir, more likely releasing a Na^+ or K^+ ion to the cytoplasm when a further monovalent cation approaches and binds to the SF of TRPM5. By contrast, Ca^{2+} ions permeate on their own, driven solely by the transmembrane electric field. Our results suggest that this mechanistic difference is what ultimately underlies the monovalent-ion selectivity in TRPM5, since the efficiency of monovalent conduction is optimised by co-operative permeation across two channel binding sites. The mechanism is subtle, and therefore the selectivity is abolished when the driving forces exceed a certain threshold, i.e., at high voltages.

Why does the inner cavity form an attractive site for monovalent cations but a repulsive site for divalent cations?

The presence of a water-filled internal cavity is a conserved feature among most cation channels, which serves to maintain a high degree of ion hydration despite its location in the centre of the lipid bilayer. As in other channels, we observe here that the major permeating species, Na^+ and K^+ ions, are re-hydrated and transiently captured in the cavity following their permeation through the SF. At higher voltages, Ca^{2+} ions can enter and traverse the cavity but do not show any deviation from their bulk hydration number during this process. At lower voltages, by contrast, Ca^{2+} ions are excluded from entering the cavity.

We therefore investigated the difference between the pore and cavity properties of the highly Ca^{2+}-selective TRP channel, TRPV5, and the monovalent-selective TRPM5. As shown in Figure 7, the general features of the pore are preserved with a constriction at the extracellular SF, a wider internal cavity region, and a second constriction at the intracellular gate. TRPM5 has a markedly shorter SF, while its cavity is wider than that of TRPV5. However, there is a substantial difference in the pore lining of the two TRP channels. Whereas the TRPV5 SF constitutes a strongly hydrophilic region, TRPM5 does not display increased hydrophilicity within its SF. The transition from the SF to the cavity is slightly hydrophobic in TRPM5, while it is a hydrophilic region in TRPV5. There are no differences between the hydrophobicity of the two channels at the intracellular gates.

We therefore attribute the monovalent-selectivity of TRPM5 to the raised hydrophobicity of its SF and upper portion of its inner cavity regions. In particular, the transition between the SF and the cavity in TRPM5 is lined by large hydrophobic Phe residues at the bottom of the SF (F904). The energetic penalty to place monovalent cations within a hydrophobic region is much smaller than for divalent cations. As observed in the simulations under increased voltage, the protein matrix does not form favourable interactions with Ca^{2+} ions in this area, which could serve to replace water molecules in their hydration shell. Accordingly, this region is identical to the position along the pore axis at which Ca^{2+} ions are repelled back into the extracellular space at lower voltages. At supra-physiological voltages, however, the increased force acting on the divalent Ca^{2+} ions is sufficient to drag some of the ions across the SF and inner cavity along with their complete hydration shell. The permeating Ca^{2+} ions do not display any noticeable interaction with protein residues during this process, which indicates that this effect is mainly driven by the strong electric field across the membrane under these conditions.

Discussion

The calculated conductances and ion selectivities we observed in our *in silico* electrophysiology simulations of TRPM5 are in good agreement with published *in vitro* values. In particular, in simulations of an equimolar mixture of NaCl and $CaCl_2$ under bio-mimetic voltages, our simulations model the impermeability of TRPM5 to divalent cations. This selectivity is even more remarkable when one considers that this selectivity was captured with a 1:1 ratio of Na^+:Ca^{2+} ions in these simulations, compared to the *in vivo* ratio of $\sim$ 112:1 ***Hurwitz*** (***1996***). To our best knowledge, the simulations reported herein represent the first *in silico* study of the ion permeation mechanism in

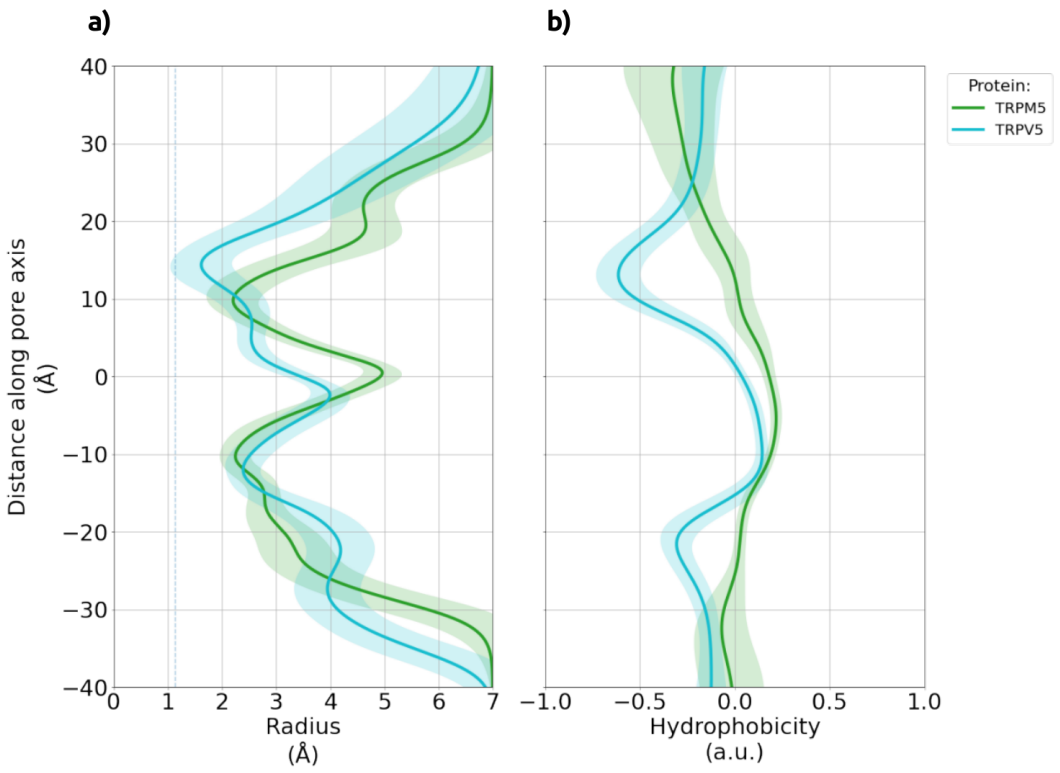

Figure 7. Pore architecture of the monovalent-selective TRPM5 channel (*green*) and the Ca^{2+}-selective TRPV5 channel (*cyan*) from MD simulations. The average pore radius (***a)***) and hydrophobic profile (***b)***) for each channel was calculated using CHAP ***Rao et al.*** (***2019***). The standard deviation is shown as shaded regions. The profile of the TRPV5 was generated from simulation data published by ***Ives et al.*** (***2022***).

any TRPM channel.

However, when the voltage of these simulations is increased to supra-physiological voltages we see a loss in the selectivity of TRPM5. A similar effect has previously been described in simulations of TRPV channels ***Ives et al.*** (***2022***). Our findings show how the increased forces acting on divalent cations at these increased voltages are sufficient to enable them to traverse energetically unfavourable regions of the pore. As a result, these findings pose a crucial question for deciding on a voltage for *in silico* electrophysiology experiments, revealing subtleties in the trade-off between the improved sampling of increased conductances and the correct recovery of ionic selectivity.

Our simulations identify two shallow, broad ion binding sites for monovalent cations in the TRPM5 channel; one within the EPV above the SF, and a second within the pore cavity, whereas divalent cations do not interact favourably within the cavity. The application of SSI has been previously used to quantify co-operative, knocking events in ion permeation mechanisms ***Ives et al.*** (***2022***). Application of this methodology identified that a knock-on mechanism is occurring between monovalent ions within this region. This co-operative mechanism between ion binding and unbinding events at adjacent binding sites facilitates enhanced permeation rates ***Hille*** (***2001***).

On the other hand, divalent cations permeate on their own, driven solely by the transmembrane voltage. At physiological voltages, this is not sufficient to permit permeation. We attribute the

energetic unfavourability of Ca^{2+} ions within the TRPM5 pore due to increased hydrophobicity of the SF and upper portion of the pore cavity.

Moreover, numerous closed-state structures of TRPM4, a close homologue of TRPM5, have been published within the PDB. Several of these structures include Na^{+} cations that have been modelled within the pore cavity ***Guo et al.*** (***2017***); ***Duan et al.*** (***2018***). Consequently, these structures (PDB: 6BCJ, 6BCL, and 6BWI) suggest that the presence of a broad monovalent cation binding site is a conserved feature among TRPM4 and TRPM5 channels.

As additional open-state structures of other TRPM channels and different orthologues are solved and published, it will be possible to further test this permeation mechanism. Additional *in silico* electrophysiological experiments of TRPM4, the other monovalent-selective TRPM channel, and of non-selective TRPM channels will facilitate a better understanding of cation permeation across the TRPM family.

In conclusion, we report that monovalent cations permeate through the pore of TRPM5 via a co-operative, distant knock-on mechanism between a binding site in the EPV and a binding site in the pore cavity. The channel, however, is impermeable to divalent cations at physiological voltages, as they experience an energetic barrier within the pore cavity, thus disrupting the co-operative permeation mechanism. We suggest that this difference in co-operativity mechanistically explains the monovalent cation-selectivity of the TRPM5 channel.

Acknowledgments

We thank the University of Dundee I.T. services for maintenance of the School of Life Sciences high-performance computing (HPC) cluster which was utilised in this research. This preprint was created using the LaPreprint template (https://github.com/roaldarbol/lapreprint) by Mikkel Roald-Arbøl.

Author contributions

CMI and UZ conceived the idea and designed the computational study, CMI conducted the simulations, CMI analysed the simulation data, NJT analysed the SSI data, UZ supervised the work, CMI and UZ wrote the manuscript with contributions from NJT, and all authors edited and reviewed the manuscript.

References

Abraham MJ, Murtola T, Schulz R, Páll S, Smith JC, Hess B, Lindahl E. GROMACS: High performance molecular simulations through multi-level parallelism from laptops to supercomputers. SoftwareX. 2015; 1-2:19–25. doi: 10.1016/j.softx.2015.06.001.

Aksimentiev A, Schulten K. Imaging α-Hemolysin with Molecular Dynamics: Ionic Conductance, Osmotic Permeability, and the Electrostatic Potential Map. Biophysical Journal. 2005; 88:3745–3761. doi: https://doi.org/10.1529/biophysj.104.058727.

Antonides LH, Hurst QW, Ives CM, Ramberg K, Ostrovitsa N, Scanlan E, Caffrey M, Pitt SJ, Zachariae U. The SARS-CoV-2 envelope (E) protein forms a calcium- and voltage-activated calcium channel. bioRxiv. 2022; doi: 10.1101/2022.10.11.511775.

Bauer P, Hess B, Lindahl E, GROMACS 2022 Source code; 2022. doi: 10.5281/zenodo.6103835.

Brixel LR, Monteilh-Zoller MK, Ingenbrandt CS, Fleig A, Penner R, Enklaar T, Zabel BU, Prawitt D. TRPM5 regulates glucose-stimulated insulin secretion. Pflügers Archive - European Journal of Physiology. 2010; 460:69–76.

Colsoul B, Schraenen A, Lemaire K, Quintens R, Van Lommel L, Segal A, Owsianik G, Talavera K, Voets T, Margolskee RF, et al. Loss of high-frequency glucose-induced Ca2+ oscillations in pancreatic islets correlates with impaired glucose tolerance in Trpm5-/- mice. Proceedings of the National Academy of Sciences. 2010; 107:5208–5213.

Darden T, York D, Pedersen L. Particle mesh Ewald: An N·log(N) method for Ewald sums in large systems. The Journal of Chemical Physics. 1993; 98:10089–10092. doi: 10.1063/1.464397.

Duan J, Li Z, Li J, Santa-Cruz A, Sanchez-Martinez S, Zhang J, Clapham DE. Structure of full-length human TRPM4. Proceedings of the National Academy of Sciences. 2018; 115:2377–2382.

Evans DJ, Holian BL. The Nose-Hoover thermostat. The Journal of Chemical Physics. 1985; 83:4069–4074. doi: 10.1063/1.449071.

van Goor MK, de Jager L, Cheng Y, van der Wijst J. High-resolution structures of transient receptor potential vanilloid channels: Unveiling a functionally diverse group of ion channels. Protein Science. 2020; 29:1569–1580.

Gowers R, Linke M, Barnoud J, Reddy T, Melo M, Seyler S, Domański J, Dotson D, Buchoux S, Kenney I, Beckstein O. MDAnalysis: A Python Package for the Rapid Analysis of Molecular Dynamics Simulations. In: *Proceedings of the 15th Python in Science Conference*; 2016. p. 98–105. doi: 10.25080/majora-629e541a-00e.

Guo J, She J, Zeng W, Chen Q, Bai Xc, Jiang Y. Structures of the calcium-activated, non-selective cation channel TRPM4. Nature. 2017; 552:205–209.

Hess B, Bekker H, Berendsen HJC, Fraaije JGEM. LINCS: A Linear Constraint Solver for molecular simulations. Journal of Computational Chemistry. 1997; 18:1463–1472. doi: 10.1002/(sici)1096-987x(199709)18:12<1463::aid-jcc4>3.0.co;2-h.

Hille B. Ion channels of excitable membranes. 3rd. ed. Sunderland, MA :; 2001.

Hilton JK, Kim M, Van Horn WD. Structural and Evolutionary Insights Point to Allosteric Regulation of TRP Ion Channels. Accounts of Chemical Research. 2019; p. acs.accounts.9b00075. doi: 10.1021/acs.accounts.9b00075.

Hofmann T, Chubanov V, Gudermann T, Montell C. TRPM5 is a voltage-modulated and Ca2+-activated monovalent selective cation channel. Current Biology. 2003; 13:1153–1158.

Huang J, Rauscher S, Nawrocki G, Ran T, Feig M, De Groot BL, Grubmüller H, MacKerell AD. CHARMM36m: An improved force field for folded and intrinsically disordered proteins. Nature Methods. 2016; 14:71–73. doi: 10.1038/nmeth.4067.

Hunter JD. Matplotlib: A 2D graphics environment. Computing in Science and Engineering. 2007; 9:99–104. doi: 10.1109/mcse.2007.55.

Hurwitz S. Homeostatic control of plasma calcium concentration. Critical Reviews in Biochemistry and Molecular Biology. 1996; 31:41–100.

Ives CM, Thomson NJ, Zachariae U. A co-operative knock-on mechanism underpins Ca^{2+}-selective cation permeation in TRPV channels. bioRxiv. 2022; doi: 10.1101/2022.04.01.486690.

Jo S, Cheng X, Islam SM, Huang L, Rui H, Zhu A, Lee HS, Qi Y, Han W, Vanommeslaeghe K, MacKerell AD, Roux B, Im W. CHARMM-GUI PDB manipulator for advanced modeling and simulations of proteins containing nonstandard residues. Advances in Protein Chemistry and Structural Biology. 2014; 96:235–265. doi: 10.1016/bs.apcsb.2014.06.002.

Jo S, Kim T, Im W. Automated builder and database of protein/membrane complexes for molecular dynamics simulations. PLoS ONE. 2007; 2. doi: 10.1371/journal.pone.0000880.

Jo S, Kim T, Iyer VG, Im W. CHARMM-GUI: A web-based graphical user interface for CHARMM. Journal of Computational Chemistry. 2008; 29:1859–1865. doi: 10.1002/jcc.20945.

Jorgensen WL, Chandrasekhar J, Madura JD, Impey RW, Klein ML. Comparison of simple potential functions for simulating liquid water. The Journal of Chemical Physics. 1983; 79:926–935. doi: 10.1063/1.445869.

Khalil M, Alliger K, Weidinger C, Yerinde C, Wirtz S, Becker C, Engel MA. Functional role of transient receptor potential channels in immune cells and epithelia. Frontiers in Immunology. 2018; 9:174.

Koivisto AP, Belvisi MG, Gaudet R, Szallasi A. Advances in TRP channel drug discovery: From target validation to clinical studies. Nature Reviews Drug Discovery. 2022; 21:41–59.

Kopec W, Köpfer DA, Vickery ON, Bondarenko AS, Jansen TLC, de Groot BL, Zachariae U. Direct knock-on of desolvated ions governs strict ion selectivity in K^+ channels. Nature Chemistry. 2018; 10:813–820. doi: 10.1038/s41557-018-0105-9.

Köpfer DA, Song C, Gruene T, Sheldrick GM, Zachariae U, De Groot BL. Ion permeation in K^+ channels occurs by direct Coulomb knock-on. Science. 2014; 346:352–355. doi: 10.1126/science.1254840.

Kutzner C, Grubmüller H, de Groot B, Zachariae U. Computational Electrophysiology: The Molecular Dynamics of Ion Channel Permeation and Selectivity in Atomistic Detail. Biophysical Journal. 2011; 101:809–817. doi: https://doi.org/10.1016/j.bpj.2011.06.010.

Kutzner C, Köpfer DA, Machtens JP, de Groot BL, Song C, Zachariae U. Insights into the function of ion channels by computational electrophysiology simulations. Biochimica et Biophysica Acta (BBA) - Biomembranes. 2016; 1858:1741–1752. doi: https://doi.org/10.1016/j.bbamem.2016.02.006.

Lee J, Cheng X, Swails JM, Yeom MS, Eastman PK, Lemkul JA, Wei S, Buckner J, Jeong JC, Qi Y, Jo S, Pande VS, Case DA, Brooks CL, MacKerell AD, Klauda JB, Im W. CHARMM-GUI Input Generator for NAMD, GROMACS, AMBER, OpenMM, and CHARMM/OpenMM Simulations Using the CHARMM36 Additive Force Field. Journal of Chemical Theory and Computation. 2016; 12:405–413. doi: 10.1021/acs.jctc.5b00935.

Lindahl, Abraham, Hess, van der Spoel, GROMACS 2020.2 Source code; 2020. doi: 10.5281/zenodo.3773801.

Liu C, Song C. Calcium binding and permeation in TRPV channels: insights from molecular dynamics simulations. bioRxiv. 2022; doi: 10.1101/2022.09.07.506889.

Liu C, Zhang A, Yan N, Song C. Atomistic details of charge/space competition in the Ca2+selectivity of ryanodine receptors. Journal of Physical Chemistry Letters. 2021 may; 12:4286–4291. doi: 10.1021/acs.jpclett.1c00681.

Lomize MA, Pogozheva ID, Joo H, Mosberg HI, Lomize AL. OPM database and PPM web server: Resources for positioning of proteins in membranes. Nucleic Acids Research. 2012; 40:370–376. doi: 10.1093/nar/gkr703.

Marcus Y. Thermodynamics of solvation of ions. Part 5.—Gibbs free energy of hydration at 298.15 K. Journal of the Chemical Society, Faraday Transactions. 1991; 87:2995–2999.

McClendon CL, Friedland G, Mobley DL, Amirkhani H, Jacobson MP. Quantifying correlations between allosteric sites in thermodynamic ensembles. Journal of Chemical Theory and Computation. 2009 sep; 5:2486–2502. doi: 10.1021/ct9001812.

Michaud-Agrawal N, Denning EJ, Woolf TB, Beckstein O. MDAnalysis: A toolkit for the analysis of molecular dynamics simulations. Journal of Computational Chemistry. 2011; 32:2319–2327. doi: 10.1002/jcc.21787.

Millman KJ, Aivazis M, Python for scientists and engineers; 2011. doi: 10.1109/mcse.2011.36.

Moran MM. TRP Channels as Potential Drug Targets. Annual Review of Pharmacology and Toxicology. 2018 jan; 58:309–330. doi: 10.1146/annurev-pharmtox-010617-052832.

Nilius B. TRP channels in disease. Biochimica et Biophysica Acta (BBA) - Molecular Basis of Disease. 2007; 1772:805–812.

Nilius B, Owsianik G. The transient receptor potential family of ion channels. Genome Biology. 2011; 12:1–11.

Oliphant TE. Python for scientific computing. Computing in Science and Engineering. 2007; 9:10–20. doi: 10.1109/mcse.2007.58.

Owsianik G, Talavera K, Voets T, Nilius B. Permeation And Selectivity Of TRP Channels. Annual Review of Physiology. 2006; 68:685–717. doi: 10.1146/annurev.physiol.68.040204.101406.

Parrinello M, Rahman A. Polymorphic transitions in single crystals: A new molecular dynamics method. Journal of Applied Physics. 1981; 52:7182–7190. doi: 10.1063/1.328693.

Pérez CA, Huang L, Rong M, Kozak JA, Preuss AK, Zhang H, Max M, Margolskee RF. A transient receptor potential channel expressed in taste receptor cells. Nature Neuroscience. 2002; 5:1169–1176.

Pérez F, Granger BE. IPython: A system for interactive scientific computing. Computing in Science and Engineering. 2007; 9:21–29. doi: 10.1109/mcse.2007.53.

Pethel SD, Hahs DW. Exact Test of Independence Using Mutual Information. Entropy. 2014; 16:2839–2849. doi: 10.3390/e16052839.

Prawitt D, Monteilh-Zoller MK, Brixel L, Spangenberg C, Zabel B, Fleig A, Penner R. TRPM5 is a transient Ca2+-activated cation channel responding to rapid changes in [Ca2+] i. Proceedings of the National Academy of Sciences. 2003; 100:15166–15171.

Ramsey IS, Delling M, Clapham DE. An introduction to TRP channels. Annual Review of Physiology. 2006; 68:619–666. doi: 10.1146/annurev.physiol.68.040204.100431.

Rao S, Sansom MSPP, Tucker SJ, Klesse G, Rao S, Sansom MSPP, Tucker SJ, Klesse G. CHAP: A Versatile Tool for the Structural and Functional Annotation of Ion Channel Pores. Journal of Molecular Biology. 2019 aug; 431:3353–3365. doi: 10.1016/j.jmb.2019.06.003.

Roux B. Ion channels and ion selectivity. Essays in Biochemistry. 2017; 61:201–209.

Ruan Z, Haley E, Orozco IJ, Sabat M, Myers R, Roth R, Du J, Lü W. Structures of the TRPM5 channel elucidate mechanisms of activation and inhibition. Nature Structural and Molecular Biology. 2021 jul; 28:604–613. doi: 10.1038/s41594-021-00607-4.

Samanta A, Hughes TE, Moiseenkova-Bell VY. Transient receptor potential (TRP) channels. Membrane Protein Complexes: Structure and Function. 2018; p. 141–165.

Schackert FK, Biedermann J, Abdolvand S, Minniberger S, Song C, Plested AJR, Carloni P, Sun H. Mechanism of calcium permeation in a glutamate receptor ion channel. ChemRxiv. 2022; doi: 10.26434/chemrxiv-2022-x73hl-v2.

Thomson NJ, Vickery ON, Ives CM, Zachariae U. Ion-water coupling controls class A GPCR signal transduction pathways. bioRxiv. 2021; doi: 10.1101/2020.08.28.271510.

Ullrich ND, Voets T, Prenen J, Vennekens R, Talavera K, Droogmans G, Nilius B. Comparison of functional properties of the Ca2+-activated cation channels TRPM4 and TRPM5 from mice. Cell Calcium. 2005; 37:267–278.

Van Der Walt S, Colbert SC, Varoquaux G. The NumPy array: A structure for efficient numerical computation. Computing in Science and Engineering. 2011; 13:22–30. doi: 10.1109/mcse.2011.37.

Vennekens R, Mesuere M, Philippaert K. TRPM5 in the battle against diabetes and obesity. Acta Physiologica. 2018; 222:e12949.

Vögele M, Thomson NJ, Truong ST, McAvity J, Zachariae U, Dror RO. Systematic Analysis of Biomolecular Conformational Ensembles with PENSA. arXiv. 2022; .

Waskom M, Botvinnik O, O'Kane D, Hobson P, Ostblom J, Lukauskas S, Gemperline DC, Augspurger T, Halchenko Y, Cole JB, Warmenhoven J, de Ruiter J, Pye C, Hoyer S, Vanderplas J, Villalba S, Kunter G, Quintero E, Bachant P, Martin M, et al., mwaskom/seaborn: v0.9.0 (July 2018); 2018. doi: 10.5281/zenodo.1313201.

Wu EL, Cheng X, Jo S, Rui H, Song KC, Dávila-Contreras EM, Qi Y, Lee J, Monje-Galvan V, Venable RM, Klauda JB, Im W. CHARMM-GUI membrane builder toward realistic biological membrane simulations. Journal of Computational Chemistry. 2014; 35:1997–2004. doi: 10.1002/jcc.23702.

Zhang A, Yu H, Liu C, Song C. The Ca^{2+} permeation mechanism of the ryanodine receptor revealed by a multi-site ion model. Nature Communications. 2020; 11:922. doi: 10.1038/s41467-020-14573-w.

Zhang Y, Hoon MA, Chandrashekar J, Mueller KL, Cook B, Wu D, Zuker CS, Ryba NJ. Coding of sweet, bitter, and umami tastes: different receptor cells sharing similar signaling pathways. Cell. 2003; 112:293–301.

533 ## Supplementary

534 Summary of MD simulations used within this study

Table S1. Summary of CompEL simulation details of the TRPM5 channel. All simulations were conducted in a di-cationic solution of 75 mM NaCl and 75 mM $CaCl_2$. In all simulations, the Ca^{2+} cations occupying the Ca_{TMD} were modelled, and remained bound for the duration of the simulations.

Protein	TRPM5			
Structure	7MBS (698-1020)			
Force field	CHARMM36m			
Water	TIP3P			
In silico electrophysiology methodology	CompEL (anti-parallel with a 9:1 concentration gradient)			
Ion	75 mM NaCl + 75mm $CaCl_2$ 266 Na^+ (CHARMM36m) 274 Ca^{2+} (Zhang et al.) 814 Cl^- (CHARMM36m)			
Independent simulations	3	3	3	3
Total simulation time (us)	1.5	1.5	1.5	1.5
Total aggregated simulation time (us)	3	3	3	3
Ionic ratios between compartments (Extracellular : Intracellular)	239 : 27 Na^+ 239 : 35 Ca^{2+} 681 : 133 Cl^-	239 : 27 Na^+ 239 : 35 Ca^{2+} 680 : 134 Cl^-	239 : 27 Na^+ 239 : 35 Ca^{2+} 677 : 137 Cl^-	239 : 27 Na^+ 239 : 35 Ca^{2+} 673 : 141 Cl^-
Estimated voltage (mV)	-50	-130	-380	-610
Permeation events	15 Na^+ 0 Ca^{2+} 0 Cl^-	18 Na^+ 0 Ca^{2+} 0 Cl^-	32 Na^+ 19 Ca^{2+} 1 Cl^-	115 Na^+ 168 Ca^{2+} 6 Cl^-
Total number of permeation events	15	18	52	289

Table S2. Summary of external applied field simulation details of the TRPM5 channel. All simulations were conducted in a mono-cationic solution of either 150 mM NaCl, 150 mM KCl, or 150 mM $CaCl_2$. In all simulations, the Ca^{2+} cations occupying the Ca_{TMD} were modelled, and remained bound for the duration of the simulations.

Protein	TRPM5		
Structure	7MBS (698-1020)		
Force field	CHARMM36m		
Water	TIP3P		
In silico electrophysiology methodology	External applied field		
Ion	150 mM NaCl 267 Na^+ (CHARMM36m) 275 Cl^- (CHARMM36m) 4 Ca^{2+} (CHARMM36m)	150 mM KCl 267 K+ (CHARMM36m) 275 Cl^- (CHARMM36m) 4 Ca^{2+} (CHARMM36m)	150 mM $CaCl_2$ 271 Ca^{2+} (Zhang *et al.*) 542 Cl^- (CHARMM36m)
Independent simulations	3	3	3
Total simulation time (us)	0.75	0.75	0.75
Estimated voltage (mV)	-340	-340	-340
Permeation events	83 Na^+ 0 Cl^-	34 K+ 0 Cl^-	54 Ca^{2+} 0 Cl^-
Total number of permeation events	83	34	54

Protein	TRPM5			
Structure	7MBS (698-1020)			
Force field	CHARMM36m			
Water	TIP3P			
In silico electrophysiology methodology	External applied field			
Ion	150 mM NaCl 267 Na^+ (CHARMM36m) 275 Cl^- (CHARMM36m) 4 Ca^{2+} (CHARMM36m)	150 mM $CaCl_2$ 271 Ca^{2+} (Zhang et al.) 542 Cl^- (CHARMM36m)	150 mM NaCl 267 Na^+ (CHARMM36m) 275 Cl^- (CHARMM36m) 4 Ca^{2+} (CHARMM36m)	150 mM $CaCl_2$ 271 Ca^{2+} (Zhang et al.) 542 Cl^- (CHARMM36m)
Independent simulations	3	3	3	3
Total simulation time (us)	0.75	0.75	0.75	0.75
Estimated voltage (mV)	-50	-50	-200	-200
Permeation events	4 Na^+ 0 Cl^-	0 Ca^{2+} 0 Cl^-	15 Na^+ 0 Cl^-	4 Ca^{2+} 0 Cl^-
Total number of permeation events	4	0	15	4

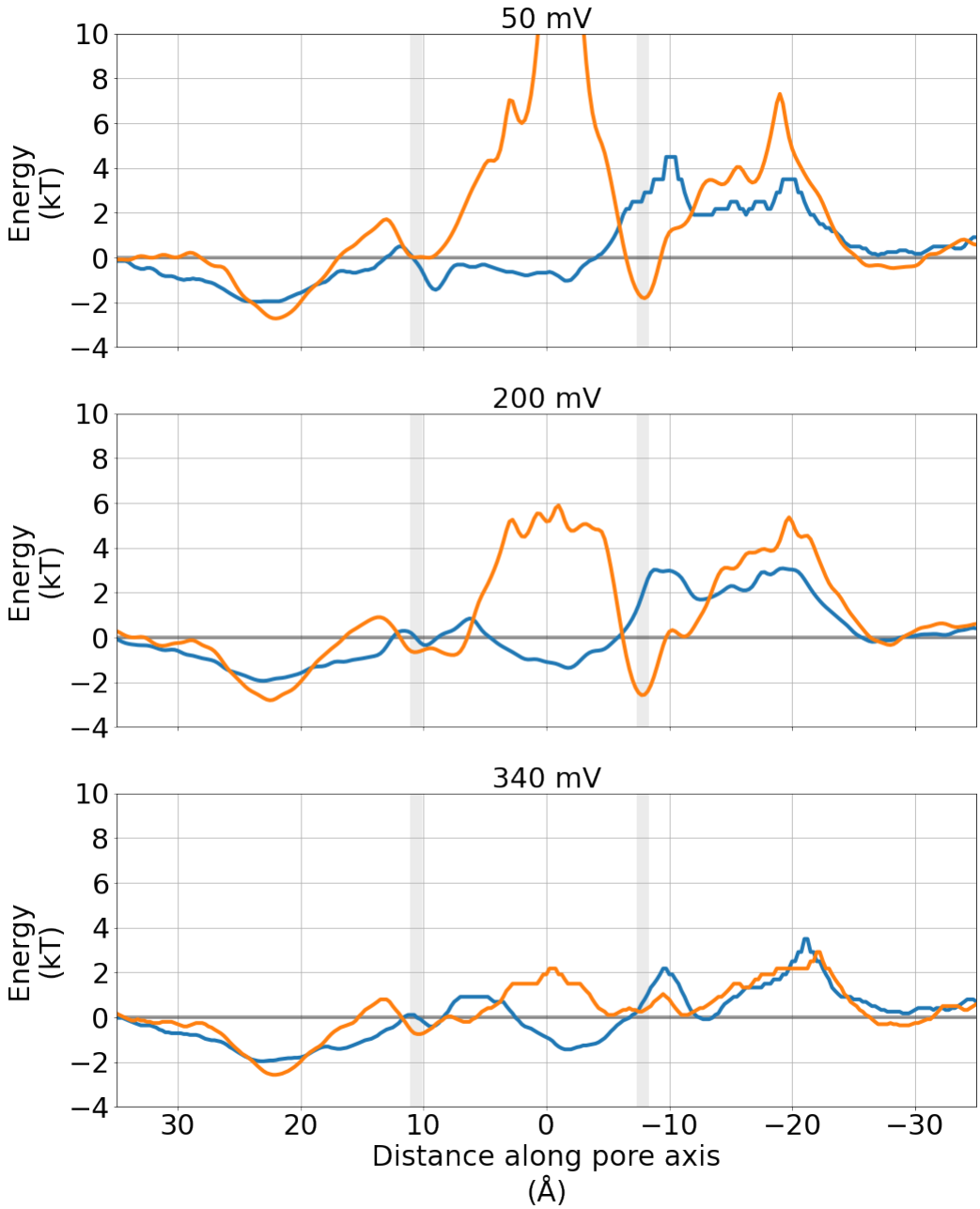

Figure S1. Negative logarithmic density profiles of permeating cations along the pore of the TRPM5 at different voltages. These simulations were performed in a mono-cationic solution, with an external applied electric field used to produce transmembrane voltages of ~ -50 mV (*top*), ~ -200 mV (*centre*), and ~ -340 mV (*bottom*). The logarithmic ion densities represent quasi-free energies (with a nominal unit of kT). The location of the pore constrictions formed by Q906 (*upper*) and I966 (*lower*) are represented as grey regions. Both plots have been smoothed using a Gaussian filter with a sigma value of 2.

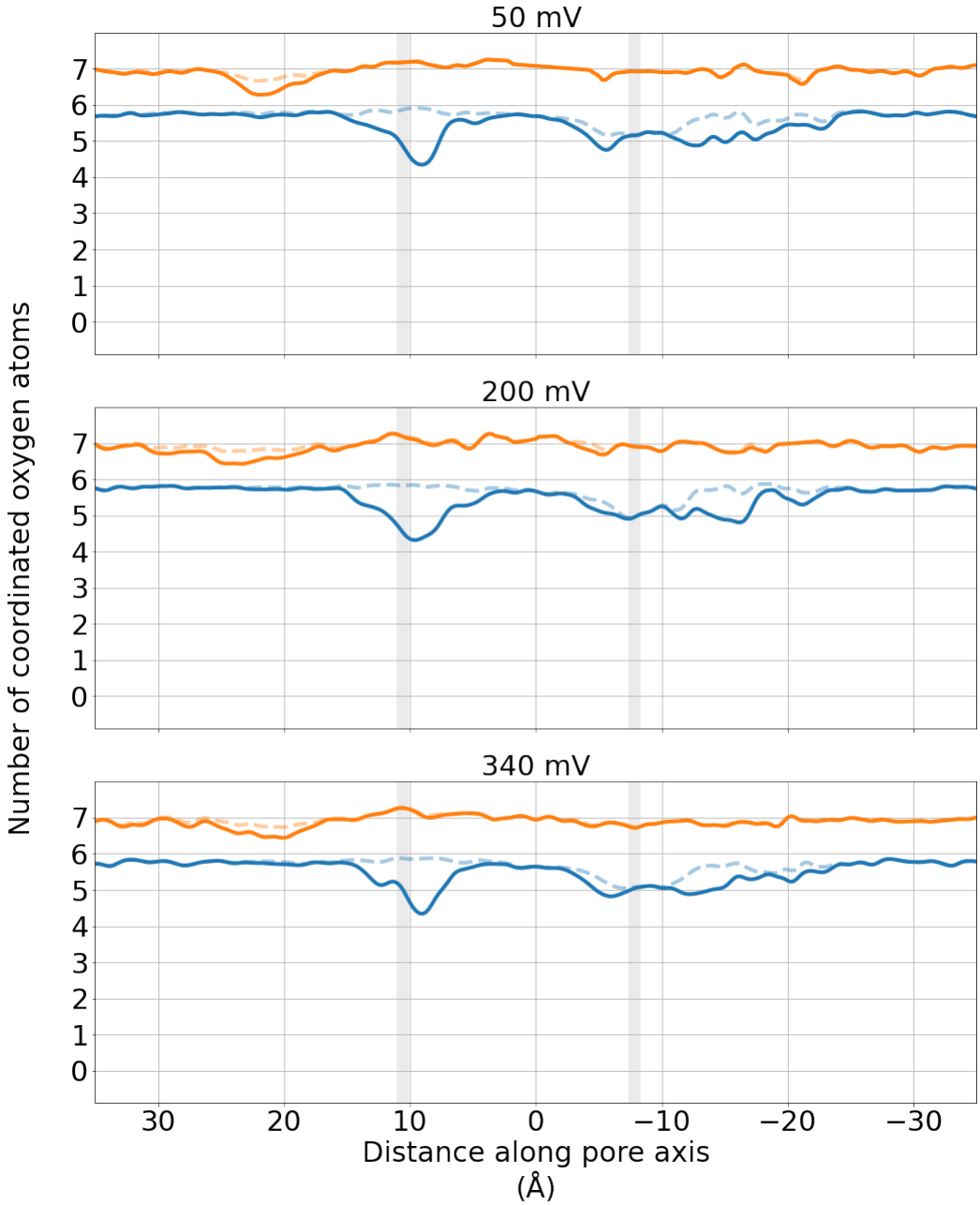

Figure S2. Solvation profiles of Na^+ (*blue*) and Ca^{2+} (*orange*) cations through the TRPM5 pore. These simulations were performed in a mono-cationic solution, with an external applied electric field used to produce transmembrane voltages of ~ -50 mV (*top*), ~ -200 mV (*centre*), and ~ -340 mV (*bottom*). The mean number of oxygen atoms of water molecules (*solid line*) and of any oxygen atoms of any molecule (*dashed line*) within 3 Å of each permeating cation is plotted. The location of the pore constrictions formed by Q906 (*upper*) and I966 (*lower*) are represented as grey regions. All plots have been smoothed using a Gaussian filter with a sigma value of 2

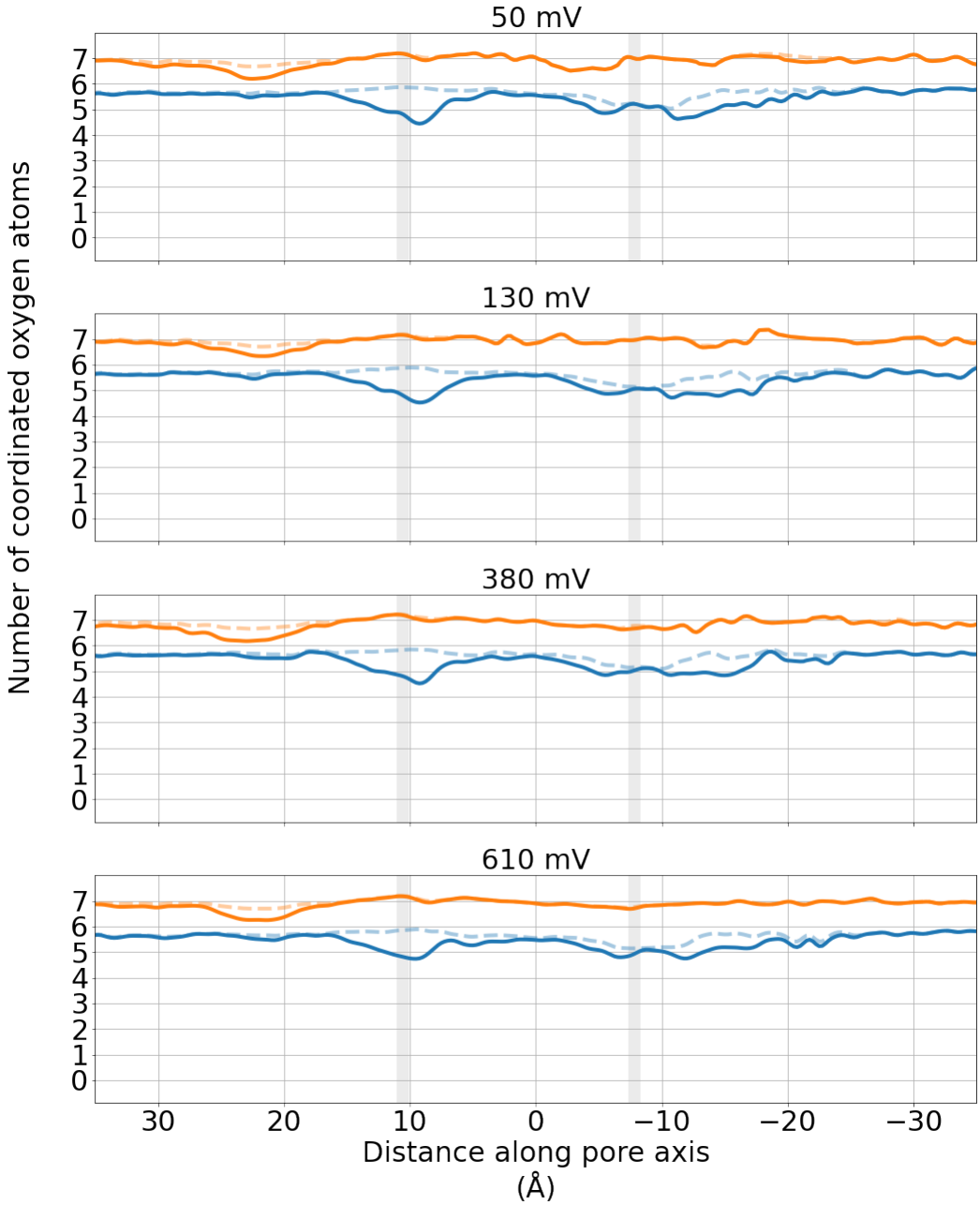

Figure S3. Solvation profiles of Na^+ (*blue*) and Ca^{2+} (*orange*) cations through the TRPM5 pore. These simulations were performed in a di-cationic solution, with the CompEL methodology used to produce transmembrane voltages of ∼ -50 mV (*top*), ∼ -130 mV (*second from top*), ∼ -380 mV (*second from bottom*), and ∼ -610 mV (*bottom*). The mean number of oxygen atoms of water molecules (*solid line*) and of any oxygen atoms of any molecule (*dashed line*) within 3 Å of each permeating cation is plotted. The location of the pore constrictions formed by Q906 (*upper*) and I966 (*lower*) are represented as grey regions. All plots have been smoothed using a Gaussian filter with a sigma value of 2.